

広島大学学術情報リポジトリ
Hiroshima University Institutional Repository

Title	Microparticles with hetero-nanointerfaces: controlled assembly of cobalt hydroxide and nickel hydroxide nanoclusters towards improved electrochemical functions
Author(s)	Tarutani, Naoki; Tokudome, Yasuaki; Jobbágy, Matías; Soler-Illia, Galo J. A. A.; Takahashi, Masahide
Citation	Journal of Materials Chemistry A , 7 : 25290 - 25296
Issue Date	2019-09-04
DOI	10.1039/C9TA07141E
Self DOI	
URL	https://ir.lib.hiroshima-u.ac.jp/00053534
Right	This is not the published version. Please cite only the published version. この論文は出版社版ではありません。引用の際には出版社版をご確認、ご利用ください。
Relation	



Microparticles with hetero-nanointerfaces: controlled assembly of cobalt hydroxide and nickel hydroxide nanoclusters towards improved electrochemical functions

Received 00th January 20xx,
Accepted 00th January 20xx

DOI: 10.1039/x0xx00000x

Naoki Tarutani,^a Yasuaki Tokudome,^{*a} Matías Jobbágy,^b Galo J. A. A. Soler-Illia^{*c} and Masahide Takahashi^a

The ultimate control of the interfaces of nanocomposite materials is essential to tailor and improve their physical/chemical properties in applications such as catalysis, or energy storage or production. Fabrication and co-assembly of a variety of nanostructured colloids is a promising way to design the interface of materials in nano-scale toward high functionality. In this study, we demonstrate a synthesis of colloids of nanocluster-sized (~ 2 nm) cobalt and nickel hydroxides and their assembly into microparticles that present hetero-nanointerfaces. Electrochemical properties were investigated to elucidate the effect of the hetero-nanointerface. Microparticles with hetero nanostructures composed of cobalt and nickel hydroxide nanoclusters revealed improved mass specific capacity (91.4 mAh/g) compared with respective microparticles with homo-nanointerface (cobalt hydroxide; 15.8 mAh/g; nickel hydroxide; 64.4 mAh/g). Further investigation suggests that the introduced hetero-nanointerface leads to lower charge transfer resistance and to improved electrochemical properties. The synthetic concept demonstrated here is expected to create unique hetero-nanointerfaces for various materials with wide-range of chemical composition towards improved and novel functionalities.

Introduction

Tailoring interfaces of materials is a promising way to obtain designed functionality, especially in the field of nanoscience and nanotechnology. A hetero-interface, junction area of two different solids, produces extraordinary electron behavior,^{1,2} which leads improvement of properties and existence of novel functionalities, for instance, electronic,^{3,4} magnetic,⁵ and catalytic⁶ properties. Using colloidal solution of nano-building blocks (NBBs) is one of the simplest and versatile pathways to controllably introduce hetero-nanointerface of materials.⁷⁻⁹

The synthesis of materials with hetero-nanointerfaces by using NBBs has been reported through evaporation-induced self-assembly process and Langmuir-Blodgett method, which shows enhanced catalytic, magnetic and optical properties.^{10,11} Recent studies have focused on using single-nm sized crystals, called nanoclusters, to design materials with significantly large hetero-interface area.^{12,13}

In general, colloidal solutions of nanoclusters were prepared through hot-injection method or non-aqueous sol-gel

process.^{14,15} In both cases, the versatilities of crystal structure and chemical composition were limited to noble metals and high-valence metal oxides because of their stability. In spite of their high potential for several applications, transition metal compound nanoclusters of low valence metal elements (Mn(II), Co(II), Ni(II), etc.) have not been yet synthesized.

We recently reported the method to control the crystallization and aggregation of transition metal hydroxides through epoxide-mediated alkanization process.¹⁶ Incorporated carboxylic acids showed multiple roles (coordination, intercalation, and adsorption) to form stable and highly dispersed metal hydroxide nanoclusters. Nanoclusters with a wide chemical composition, M(OH)₂ (M = Mn(II), Fe(II), Co(II), Ni(II), and Cu(II)), were obtained through our approach.

We here focus on the preparation of nanocomposites with a large hetero-interface area by contacting different kinds of divalent metal hydroxide nanoclusters. Electrochemically active cobalt hydroxide and nickel hydroxide were employed as a model case and illustrate the potential of this approach. Microparticles with hetero-nanointerfaces were synthesized by spray drying of a mixture of colloidal solutions of cobalt hydroxide and nickel hydroxide nanoclusters. For a comparison, homo-interfaced microparticles of cobalt hydroxide, nickel hydroxide, and cobalt-nickel mixed hydroxide (solid solution) were prepared. The effect of the introduction of the hetero-nanointerface was investigated by electrochemical measurements. The microparticles with hetero-nanointerfaces showed an improvement of electrochemical functions, the degree of which is as high as that of referential cobalt-nickel hydroxide solid solution with an atomic scale homogeneity. The

^a Department of Materials Science, Graduate School of Engineering, Osaka Prefecture University, Sakai, Osaka 599-8531, Japan. E-mail (Y. Tokudome): tokudome@mtr.osakafu-u.ac.jp

^b INQUIMAE-CONICET, Facultad Ciencias Exactas y Naturales, Universidad de Buenos Aires, Buenos Aires, C1428EHA, Argentina.

^c Instituto de Nanosistemas, Universidad Nacional de General San Martín, Av. 25 de Mayo y Francia, San Martín, 1650, Argentina. E-mail (G. J. A. A. Soler-Illia): gsoler-illia@unsam.edu.ar

Electronic Supplementary Information (ESI) available: [details of any supplementary information available should be included here]. See DOI: 10.1039/x0xx00000x

result obtained in this study implies that unique properties will be obtained by an introduction of a large hetero-interface using nanoclusters.

Experimental

Chemicals

Cobalt chloride hexahydrate ($\text{CoCl}_2 \cdot 6\text{H}_2\text{O}$, 99.0%), nickel chloride hexahydrate ($\text{NiCl}_2 \cdot 6\text{H}_2\text{O}$, 98.0%), acrylic acid (99%), ethanol (99.5%), propylene oxide (PO, > 99%), and poly(vinyl alcohol) ($M_w = 500$) were used as received. Acrylic acid and propylene oxide were purchased from Sigma-Aldrich Co. All other reagents were purchased from Wako Pure Chemicals Industries, Ltd. Ultrapure water of 18.2 $\text{M}\Omega \cdot \text{cm}$ resistivity was used in all experiments.

Synthesis of homo-nanointerfaced microparticles composed of cobalt-nickel hydroxide nanoclusters (Fig. 1a).

$\text{CoCl}_2 \cdot 6\text{H}_2\text{O}$, $\text{NiCl}_2 \cdot 6\text{H}_2\text{O}$, and acrylic acid were dissolved in ethanol. PO was added to a solution and stirred for 30 s. Resultant homogenous solutions were left at a room temperature (20–25 °C) for 60 min. The amount of $\text{CoCl}_2 \cdot 6\text{H}_2\text{O}$, $\text{NiCl}_2 \cdot 6\text{H}_2\text{O}$, acrylic acid, ethanol, and PO were x , $1-x$, 4.0, 34.3, 15.0 mmol, respectively ($0 \leq x \leq 1$). The obtained colloids, denoted as $\text{Co}_x\text{Ni}_{1-x}(\text{OH})_2$, were diluted with 10 mL of water and stirred for 1 min. Obtained solutions were spray dried using a Buchi B-290 mini spray dryer. The spray conditions were configured as follows; inlet air temperature of 150 °C, gas (air, 30 ± 5 RH%) flow of 601 L/h, peristaltic pump speed of 3 mL/min, aspirator of 35 m³/h, and resultant outlet temperature of 74–84 °C. The dried powders collected from a sample glass vessel were heat treated at 150 °C for 12 h with a vacuum condition to complete drying. The powders prepared through this process were denoted as Homo- $x:1-x$.

Synthesis of hetero-nanointerfaced microparticles composed of mixture of cobalt hydroxide nanoclusters and nickel hydroxide nanoclusters (Fig. 1b)

$\text{Co}(\text{OH})_2$ and $\text{Ni}(\text{OH})_2$ nanocluster colloids were synthesized through the above procedure in the reaction scales of y and $1-y$ times, respectively ($0 < y < 1$). Prepared $\text{Co}(\text{OH})_2$ and $\text{Ni}(\text{OH})_2$ nanocluster colloids were mixed followed by dilution with 10 mL of water. After stirred for 1 min, the obtained solutions were spray dried and oven dried with the condition same as written above section. The powders prepared through this procedure were denoted as Hetero- $y:1-y$.

Characterization

A field emission scanning microscope (SEM; S-8020, Hitachi, Japan) equipped with energy dispersed X-ray spectroscopy (EDS) was used to observe microstructure of synthesized materials. A transmission electron microscope (TEM; JEM-2100F, JEOL, Japan) was employed at an operating voltage of 200 kV to observe size and shape of nanoclusters. Powder X-ray diffraction (PXRD; Multiflex, Rigaku, Japan) using $\text{Cu K}\alpha$ radiation ($\lambda = 1.544 \text{ \AA}$) was used to characterize crystal phase and crystallite size of dried samples. X-ray photoelectron spectrometer (XPS) analyses were carried out with ESCA-5600

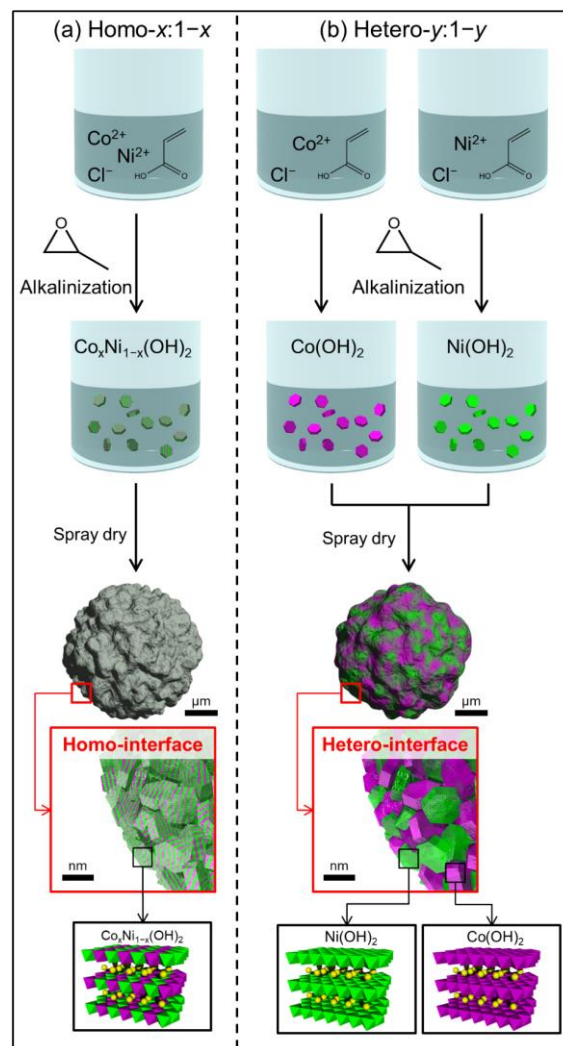


Fig. 1 Schematic illustration of synthetic pathways of (a) microparticles with homo-nanointerface (Homo- $x:1-x$) and (b) hetero-nanointerface (Hetero- $y:1-y$). Purple octahedrons, green octahedrons, and yellow spheres in the crystal structural figure depict 6-coordinated Co(II), 6-coordinated Ni(II) and acrylates, respectively.

(Ulvac-Phi, Japan) using a monochromatic Al $K\alpha$ source (200 W) to evaluate the oxidation state of Co and Ni atoms. Fourier transform infrared (FT-IR) spectroscopy (ALPHA FT-IR spectrometer, Bruker Optik GmbH, Germany) and ultraviolet-visible-near infrared (UV-Vis-NIR) spectroscopy (V-670 spectrophotometer, JASCO Corp.) were used to characterize local structure of dried sample. The small angle X-ray scattering (SAXS) measurement was performed to characterize formed particle size with the beamline of the Brazilian Synchrotron Light Laboratory (LNLS, Brazil D11A-SAXS1-18927 and 20160366). Details of characterization conditions are written in electronic supporting information (ESI).

Electrochemical measurement

All electrochemical measurements were performed by using a potentiostat with frequency response analyzer (HZ-7000 and HZA-FRA1, Hokuto Denko, Japan). The dried microparticles were dispersed in water (1.0 g/L) by ultrasonicated for 5 min. Poly(vinyl alcohol) aqueous solution (1 g/L) was added to the

suspension. The mixture was composed of 90 wt% of sample and 10 wt% of poly(vinyl alcohol). After 5 min ultrasonication, 5.56 μL of obtained solution was dropped on the Au working electrode (diameter: 5 mm), corresponding to 5.0 μg of sample. The electrode was dried in a preheated oven at 120 $^{\circ}\text{C}$ for 10 min. After cooling the electrode, cyclic voltammetry (CV), galvanostatic charge-discharge, and electrochemical impedance spectroscopy (EIS) measurements were performed. All electrochemical measurements were carried out in a conventional three-electrode cell configuration with a 1.0 mol/L KOH aqueous solution as an electrolyte at 25 $^{\circ}\text{C}$. The electrolyte was purged with N_2 at 250 mL/min for 10 min before the measurements. A platinum wire and Hg/HgO (or Ag/AgCl) were used as a counter electrode and a reference electrode, respectively. The detailed conditions of each measurement are described in ESI.

Results and discussion

Material synthesis and characterization

The addition of PO triggers pH increase by scavenging protons through ring-opening reaction with nucleophilic species.¹⁷ Along with pH increase, solid components were formed in reacting solution, which was confirmed by in-situ SAXS measurement. Fig. 2a shows the time-dependent growth of $\text{Co}(\text{OH})_2$, $\text{Ni}(\text{OH})_2$, and $\text{Co}_{0.5}\text{Ni}_{0.5}(\text{OH})_2$ nanoclusters. The diameters were estimated by fitting SAXS patterns with a unified equation^{18,19} (see experimental of ESI). The particles started to grow after addition of PO and reached a stable specific size after 60 min. The final particle diameter (1.88–2.23 nm) and growth rate (0.088–0.090 nm/min) were irrespective to the chemical composition of precursor solution (Table 1). The

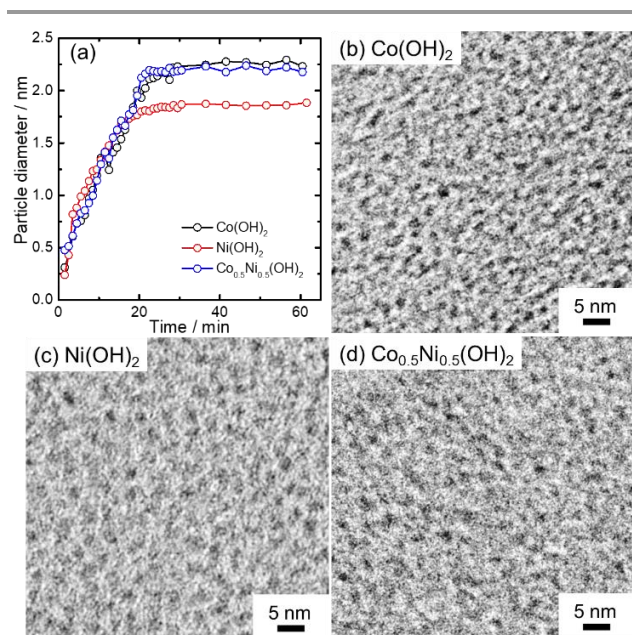


Fig. 2. (a) Time-dependent particle growth of $\text{Co}(\text{OH})_2$, $\text{Ni}(\text{OH})_2$, and $\text{Co}_{0.5}\text{Ni}_{0.5}(\text{OH})_2$ nanoclusters after addition of PO. Particle diameter was estimated from corresponding SAXS patterns. TEM images of (b) $\text{Co}(\text{OH})_2$, (c) $\text{Ni}(\text{OH})_2$ and (d) $\text{Co}_{0.5}\text{Ni}_{0.5}(\text{OH})_2$ nanoclusters after dilution with water.

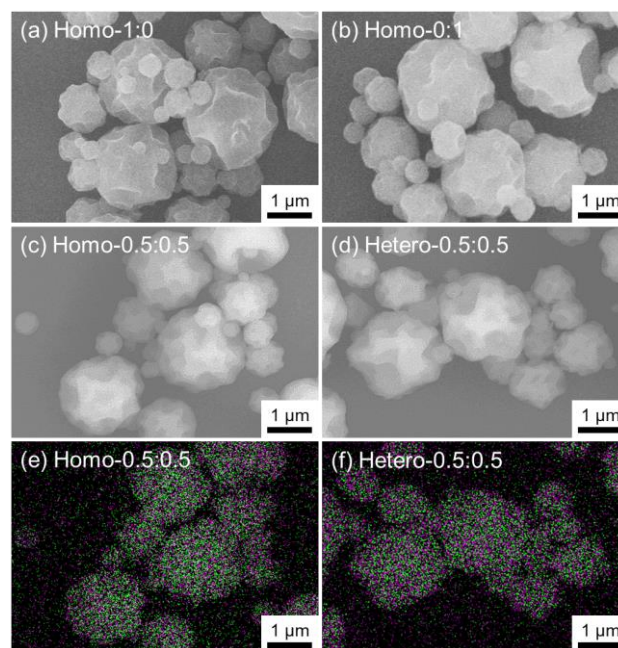


Fig. 3 (a)-(d) SEM images and (e)(f) EDS mapping images (Co: purple; Ni: green) of Homo-1:0, Homo-0:1, Homo-0.5:0.5, and Hetero-0.5:0.5.

results indicate that nanoclusters of $\text{Co}(\text{OH})_2$, $\text{Ni}(\text{OH})_2$, and $\text{Co}_{0.5}\text{Ni}_{0.5}(\text{OH})_2$ were successfully formed and stabilized in a same manner.

Fig. 2b-2d show the TEM images of $\text{Co}(\text{OH})_2$, $\text{Ni}(\text{OH})_2$, and $\text{Co}_{0.5}\text{Ni}_{0.5}(\text{OH})_2$ nanoclusters after dilution with water (before spray dry). All samples showed spherical shape with a narrow size distribution (Fig. S1). The average diameters estimated from TEM images of $\text{Co}(\text{OH})_2$, $\text{Ni}(\text{OH})_2$, and $\text{Co}_{0.5}\text{Ni}_{0.5}(\text{OH})_2$ were 1.6 nm, 1.7 nm, and 2.0 nm, respectively, which are comparable to the diameter calculated from SAXS measurement (Table 1). Equal volume of $\text{Co}(\text{OH})_2$ and $\text{Ni}(\text{OH})_2$ nanocluster colloids were mixed after 60 min reaction to prepare the precursor solution of hetero-nanointerfaced materials (0.5 $\text{Co}(\text{OH})_2$ -0.5 $\text{Ni}(\text{OH})_2$). The SAXS pattern and TEM image indicate that nanocluster colloids were successfully mixed without geometric change of objects, such as crystal growth and aggregation (Fig. S2). In spite of the small size of nanoclusters, no significant size change was observed after dilution with water, which implies nanoclusters were stable enough during synthetic process.

Powders of Homo-1:0, Homo-0:1, Homo-0.5:0.5, and Hetero-0.5:0.5 were obtained after spray drying of the corresponding nanocluster colloids. As we reported previously, layered metal hydroxides with hindered crystalline growth along ab axis are obtained by epoxide-mediated alkalization in the presence of acrylic acid.^{20,21} The PXRD patterns of the samples are shown in Fig. S3; only a main peak was detected around 8 $^{\circ}$ (lattice spacing of ~ 11.5 \AA), which indicates that layered metal hydroxides with small lateral size in *ab* axis direction were formed. Considering the reported studies,^{22,23} the peaks were assigned as 00 l plane of layered metal hydroxide intercalated with double-layer of acrylates. The crystallite sizes calculated from the 00 l peak were around 3 nm, comparable to the diameter of as-synthesized nanoclusters (Table 1).

Table 1 Particle growth rate, particle diameter of nanoclusters, crystallite sizes and Co to Ni atomic ratio.

Sample ID	v_p^a / nm min ⁻¹	d_{SAXS}^b / nm	d_{TEM}^c / nm	d_{001}^d / nm	Co:Ni ^e	Co:Ni ^f
Homo-1:0	0.088	2.2	1.6	3.1	-	-
Homo-0:1	0.090	1.9	1.7	2.9	-	-
Homo-0.5:0.5	0.090	2.2	2.0	2.8	0.51:0.49	0.52:0.48
Hetero-0.5:0.5	-	1.9	1.9	3.0	0.50:0.50	0.51:0.49

^a Particle growth rate estimated from Fig. 2a by linear fitting of 1–15 min. Particle diameter calculated from ^b SAXS patterns and ^c TEM images. ^d Crystallite size estimated from 001 peaks. Atomic ratio of Co and Ni estimated from ^e EDS and ^f XPS spectra.

Further XRD measurements performed with heat treated samples (Fig. S4). Hydroxides of Homo-1:0 and Homo-0:1 were phase transformed to Co(II)Co(III)₂O₄ and NiO/Ni, respectively, after treated at 300 °C for 2 h. NiCo₂O₄/NiO were formed in the case of Homo-0.5:0.5 like as typical Co-Ni hydroxide solid solution, whereas Hetero-0.5:0.5 form a mixture of Co(II)Co(III)₂O₄/NiO/Ni. This implies that Homo-0.5:0.5 and Hetero-0.5:0.5 have different nanointerface structures.

Polydispersed microparticles with a dimple texture were obtained in a range of 0.2–2.0 μm in diameter (Fig. 3a–3d). The diameter and shape of microparticles were identical among all samples, because those are strongly depending on the spray dry processing condition, rather than on the metal composition.²⁰ The distribution of Co and Ni elements was investigated using EDS mapping scan (Fig. 3e and 3f). Each microparticle of Homo-0.5:0.5 and Hetero-0.5:0.5 showed the signal of both Co and Ni throughout the whole set of samples, without noticeable segregation. Co/Ni molar ratios of Homo-*x*:1–*x* and Hetero-*y*:1–*y* (0 ≤ *x* ≤ 1, 0 < *y* < 1) calculated from EDS spectra were in good agreement with the nominal molar ratio (Fig. S5). The control of chemical composition enables to investigate the electrochemical, catalytic, and adsorption properties of metal hydroxides.^{24,25}

Further characterizations were performed using spectroscopic measurements to obtain information of the local

structures. XPS spectra were obtained to measure the chemical composition and oxidation state of cobalt and nickel at surface of microparticles (Fig. 4). The atomic ratios, Co:Ni, of Homo-0.5:0.5 and Hetero-0.5:0.5 samples were 0.52:0.48 and 0.51:0.49, respectively, which are comparable to EDS results indicating that nanoclusters of cobalt hydroxide and nickel hydroxide were homogeneously distributed from the surface to the core of microparticles. The difference between binding energies of Co 2p_{3/2} and Co 2p_{1/2}, and binding energies of Ni 2p_{3/2} and Ni 2p_{1/2} were 16.0 eV and 17.5–17.7 eV, respectively. These values are in good agreement with reported one for Co(II) and Ni(II) hydroxide.^{26–28} IR and UV-Vis-NIR measurements summarized that Homo-1:0, Homo-0:1, Homo-0.5:0.5, and Hetero-0.5:0.5 were all composed of octahedral six-coordinated M(OH)₆ (brucite-type arrangement) with coordinated, intercalated, and adsorbed acrylates (Fig. S6). These results indicate that synthesized materials have comparable characteristics of nanoclusters (diameter, crystallite size, crystal structure, coordination number and oxidation state) and microparticles (size distribution, morphology, and chemical compositional homogeneity).

Electrochemical measurement

Electrochemical properties were investigated using CV, galvanostatic charge-discharge, and EIS measurements. CV curve of Homo-1:0 showed two pairs of redox peaks of 117/107 mV and 387/329 mV (oxidation/reduction) (Fig. 5 and S7) corresponding to following redox reactions;²⁹

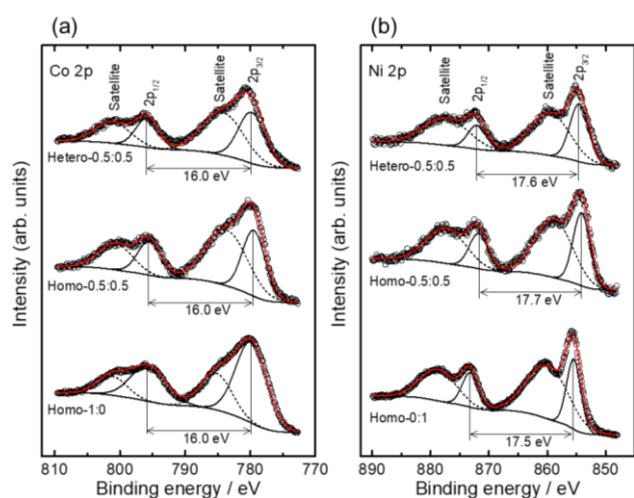
$$\text{Co(OH)}_2 + \text{OH}^- \leftrightarrow \text{CoOOH} + \text{H}_2\text{O} + \text{e}^- \quad (1)$$


Fig. 4. (a) Co 2p and (b) Ni 2p XPS spectra of Homo-1:0, Homo-0:1, Homo-0.5:0.5, and Hetero-0.5:0.5. Open circle is experimental data, black line is fitted curve (solid; 2p_{1/2} and 2p_{3/2} peak, dot; satellite peak), and red solid line is cumulative curve of fitted peaks.

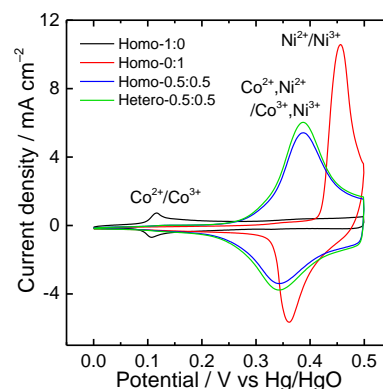
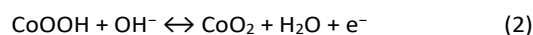
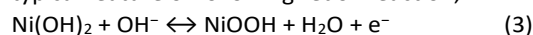


Fig. 5. CV curves of Homo-1:0, Homo-0:1, Homo-0.5:0.5, and Hetero-0.5:0.5 recorded at a scan rate of 100 mV/s.



The two peaks (455/360 mV) of CV curve of Homo-0:1 is a typical feature of following redox reaction;³⁰



CV curve of Homo-0.5:0.5 showed a set of redox peaks at intermediate potential range between those of Homo-1:0 and Homo-0:1, which is a typical feature of solid solution of cobalt-nickel hydroxides prepared via co-precipitation.^{31–33} The shift and broadening of redox peaks were explained by the existence of multiple phases composed of Co and Ni during electrochemical reaction.³⁴ Interestingly, Hetero-0.5:0.5 also shows the redox peaks comparable to Homo-0.5:0.5. On the other hands, a physical mixture of Homo-1:0 and Homo-0:1 (hetero-microinterfaced materials) did not show significant peak shift (Fig. S8). The results suggest that the introduction of relatively large hetero-interface for Hetero-0.5:0.5 leads to hybridization of functions of cobalt hydroxide and nickel hydroxide, in a similar fashion of a solid solution. Additionally, Hetero- $y:1-y$ shows the shift of redox peaks and a varying capacity as a function of chemical composition, which is also in good agreement with the trend of Homo- $x:1-x$ and solid solutions of cobalt-nickel hydroxide reported in previous studies (Fig. S9).³⁵ The introduction of this kind of hetero-nanointerface cannot be achieved by a deposition of cobalt hydroxide onto nickel hydroxide through electrodeposition, precipitation, and co-stacking of exfoliated cobalt and nickel hydroxide nanosheets.^{36–40} In the aforementioned cases, the improvement of electrochemical performance was achieved without losing original redox signals of cobalt hydroxide and nickel hydroxide, and massive hybridization was not achieved. These results successfully demonstrate that the introduction of the large hetero-nanointerface by using different types of nanoclusters is a promising strategy to design “solid-solution-like” nanocomposites.

Galvanostatic charge-discharge curves are shown in Fig. 6a. The mass specific capacities of Homo-1:0, Homo-0:1, Homo-0.5:0.5, and Hetero-0.5:0.5 were 17.4, 69.4, 87.2, 96.2 mAh/g, respectively. The mass specific capacities along with various discharge rates shown in Fig. 6b. Compared with Homo-1:0 and Homo-0:1, the capacities of Homo-0.5:0.5 and Hetero-0.5:0.5 were higher at entire discharge rates. As is reported,^{41,42} addition of Co ions within nickel hydroxide enables to form a conductive Co(III)-based compounds, which improves the inherently poor electron transfer property of Ni(III)-based compounds leading to larger capacities. Cyclic performances were tested at a constant current density of 10 A/g (Fig. 6c). The cycle performance of Homo-0.5:0.5 was better than those of Homo-1:0 and Homo-0:1. Hetero-0.5:0.5 showed an intermediate trend between Homo-1:0 and Homo-0:1; the relative capacity increases for the first 50 cycles and then decreases gradually. In spite of the incorporation of Ni(OH)₂ with a poor cycle performance, Hetero-0.5:0.5 showed a capacity comparable to initial one even after 200 cycles, implying the hetero-nanointerface contributes to achieve the robust electrochemical performance.

Although Hetero-0.5:0.5 showed the largest capacity, its estimated electrochemical surface area, C_{dl} , stands at an

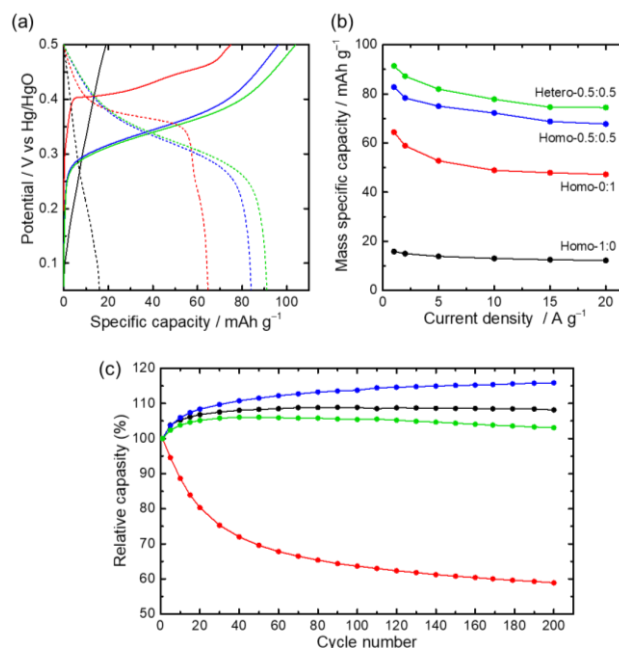


Fig. 6 (a) Galvanostatic charge (solid line) and discharge (dot line) curves recorded at a current density of 1 A/g, (b) mass specific capacity dependence with current density and (c) cycle performance recorded at a constant current density of 10 A/g of Homo-1:0 (black), Homo-0:1 (red), Homo-0.5:0.5 (blue) and Hetero-0.5:0.5 (green).

intermediate value (Table 2). To clarify a contributing factor toward a large capacity, EIS were recorded (Fig. 7). The semicircle in high frequency region is composed of solution resistance (R_s), charge transfer resistance (R_{ct}), constant phase elements (CPE-1 and CPE-2). The Warburg impedance (Z_w) corresponds to the straight line in the low frequency region. The calculated kinetic parameters were listed in Table 2. The R_s were comparable value among all samples. The R_{ct} of Hetero-0.5:0.5 was 0.659 Ω , which considerably small compared with the R_{ct} of Homo-1:0 (11.7 Ω), Homo-0:1 (5.48 Ω), and Homo-0.5:0.5 (1.08 Ω). Z_w of Homo-0.5:0.5 and Hetero-0.5:0.5 were smaller than those of Homo-1:0 and Homo-0:1. This indicates that the diffusion of OH⁻ is enhanced for both Homo-0.5:0.5 and Hetero-0.5:0.5. CPE-1 of Homo-1:0 and Homo-0:1 were 0.825 and 0.739 corresponding to a pseudocapacitive feature. On the other hand, CPE-2 of all the samples were refined as 0.957–1.00 corresponding to an ideal capacitor. The low resistance derived from hetero-nanointerface may improve the diffusion of electrons leading a large specific capacity.

In summary, improvement of electrochemical properties will be obtained by an introduction of large hetero-interface area using nanoclusters. The importance of hetero-interface has been discussed in the case of not only hydroxides but also wide variety of compounds, such as metals, oxides, sulphides, and nitrides.^{43–45} Considering these, the advantage of the concept in this study lies in the control of chemical composition beyond the limitations imposed by the coprecipitation of solid solutions. For instance, although complex solid solution nanocrystals (composed of more than 5 elements) is desired due to their high electrochemical catalytic activities, it is still

challenging to prevent phase segregation and crystallization.⁴⁶
We believe that

Table 2 A summary of electrochemical characteristic parameters obtained from equivalent circuit model

Sample ID	C_m^a	C_{dl}^b	R_s	R_{ct}	Z_w	CPE-1 ^c		CPE-2 ^c	
	/ mAh g ⁻¹	/ μF cm ⁻²	/ Ω	/ Ω	/ Ω	p	$T / 10^{-4} \text{ F s}^{p-1}$	p	$T / 10^{-3} \text{ F s}^{p-1}$
Homo-1:0	15.8	187	6.93	11.7	93.9	0.825	1.78	1.00	0.405
Homo-0:1	64.4	48.9	6.15	5.48	95.8	0.739	4.49	0.981	1.14
Homo-0.5:0.5	82.8	74.8	6.47	1.08	37.2	1.00	0.142	0.957	4.07
Hetero-0.5:0.5	91.4	74.5	6.03	0.659	32.7	1.00	0.159	0.964	4.40

^a: mass specific capacities calculated from discharge curves at a current density of 1 A/g. ^b: double layer capacitance estimated from linear fitting of scan rate versus charge currents plot, which shows linear proportion to electrochemical surface area. ^c: CPE is the constant phase element. The impedance of CPE is $1/(j\omega)^p T$, where j is imaginary unit, ω is angular frequency, p is CPE exponent, and T is CPE constant.

the materials with unique functionalities will be found by introducing a large hetero-interface using a variety of nanoclusters.

Conclusions

Cobalt hydroxide, nickel hydroxide and cobalt-nickel hydroxide solid solution nanoclusters (~ 2 nm) were prepared through epoxide-mediated alkalization in the presence of acrylic acid as a size-control agent. The different nanocluster colloids were successfully mixed without crystal growth or aggregation. Owing to the stable characteristic of nanoclusters in water, spherical microparticles with a hetero-nanointerface or homo-nanointerface were obtained by spray drying the colloidal suspensions. The hetero-nanointerfaced microparticles composed of cobalt hydroxide and nickel hydroxide nanoclusters showed improved electrochemical properties compared with homo-nanointerfaced counterparts. Our results suggest that there is a synergy between the properties of the individual nanoclusters originated from the large hetero-interface area originated in the nanocluster mixture. The synthetic approach shown here potentially allows the fabrication of materials with chemical composition beyond

the limitation of solid solution system and lead existence of a unique functionalities. In addition, the versatile method of synthesis of highly dispersible and stable nanoclusters permits to envisage a library of transition metal (hydr)oxide clusters. These stable nano-building blocks allows an easy to carry high throughput combinatorial screening. This concept can be extended to diverse aspects beyond the discussed herein, giving rise to nanocomposites bearing complex and tailorable bulk and surface features that will permit to finely control their catalytic, optical, electronic, magnetic, ion exchange or charge storage behaviour.

Conflicts of interest

There are no conflicts to declare.

Acknowledgements

Strategic Young Researcher Overseas Visits Program for Accelerating Brain Circulation from JSPS is gratefully acknowledged. The present work is partially supported by JSPS KAKENHI, LNLS proposal SAXS1 18927, ANPCyT (PICT 2087), UBACyT (20020130100610BA), Izumi Science and Technology Foundation (H29-J-130) and the Foundation for the Promotion of Ion Engineering.

Notes and references

- 1 A. Ohtomo and H. Y. Hwang, *Nature*, 2004, **427**, 423–426.
- 2 N. Reyren, S. Thiel, A. D. Caviglia, L. F. Kourkoutis, G. Hammerl, C. Richter, C. W. Schneider, T. Kopp, A.-S. Ruetschi, D. Jaccard, M. Gabay, D. A. Muller, J.-M. Triscone and J. Mannhart, *Science (80-.)*, 2007, **317**, 1196–1199.
- 3 Q. Zheng, W. A. Saidi, Y. Xie, Z. Lan, O. V. Prezhdo, H. Petek and J. Zhao, *Nano Lett.*, 2017, **17**, 6435–6442.
- 4 Z. Lian, M. Sakamoto, H. Matsunaga, J. J. M. Vequizo, A. Yamakata, M. Haruta, H. Kurata, W. Ota, T. Sato and T. Teranishi, *Nat. Commun.*, 2018, **9**, 1–7.
- 5 H. Yan, Z. Zhang, S. Wang, X. Wei, C. Chen and K. Jin, *ACS Appl. Mater. Interfaces*, 2018, **10**, 14209–14213.

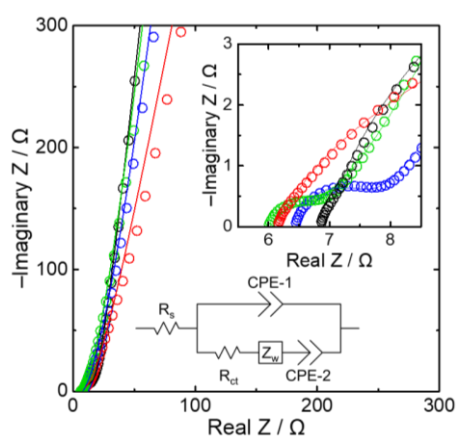


Fig. 7. EIS of Homo-1:0 (black), Homo-0:1 (red), Homo-0.5:0.5 (blue) and Hetero-0.5:0.5 (green) (open circle: experimental data, solid lines: fitted data). Inset is focused on high frequency range.

- 6 Y. Yamada, C. K. Tsung, W. Huang, Z. Huo, S. E. Habas, T. Soejima, C. E. Aliaga, G. A. Somorjai and P. Yang, *Nat. Chem.*, 2011, **3**, 372–376.
- 7 J. Henzie, M. Grünwald, A. Widmer-Cooper, P. L. Geissler and P. Yang, *Nat. Mater.*, 2012, **11**, 131–137.
- 8 Y. Xu, M. P. Konrad, W. W. Y. Lee, Z. Ye and S. E. J. Bell, *Nano Lett.*, 2016, **16**, 5255–5260.
- 9 J. J. Armao IV, I. Nyrkova, G. Fuks, A. Osypenko, M. Maaloum, E. Moulin, R. Arenal, O. Gavat, A. Semenov and N. Giuseppone, *J. Am. Chem. Soc.*, 2017, **139**, 2345–2350.
- 10 M. Osada and T. Sasaki, *J. Mater. Chem.*, 2009, **19**, 2503–2511.
- 11 M. Osada and T. Sasaki, *Adv. Mater.*, 2012, **24**, 210–228.
- 12 S. Zhao, R. Jin, H. Abroshan, C. Zeng, H. Zhang, S. D. House, E. Gottlieb, H. J. Kim, J. C. Yang and R. Jin, *J. Am. Chem. Soc.*, 2017, **139**, 1077–1080.
- 13 M. Nakaya, T. Iwasa, H. Tsunoyama, T. Eguchi and A. Nakajima, *Adv. Funct. Mater.*, 2014, **24**, 1202–1210.
- 14 C. B. Murray, D. J. Norris and M. G. Bawendi, *J. Am. Chem. Soc.*, 1993, **115**, 8706–8715.
- 15 M. Niederberger, *Acc. Chem. Res.*, 2007, **40**, 793–800.
- 16 N. Tarutani, Y. Tokudome, M. Jobbágy, F. A. Viva, G. J. A. A. Soler-Illia and M. Takahashi, *Chem. Mater.*, 2016, **28**, 5606–5610.
- 17 A. E. Gash, T. M. Tillotson, J. H. Satcher, J. F. Poco, L. W. Hrubesh and R. L. Simpson, *Chem. Mater.*, 2001, **13**, 999–1007.
- 18 G. Beaucage and D. W. Schaefer, *J. Non. Cryst. Solids*, 1994, **172–174**, 797–805.
- 19 G. Beaucage, *J. Appl. Crystallogr.*, 1995, **28**, 717–728.
- 20 N. Tarutani, Y. Tokudome, M. Jobbágy, G. J. A. A. Soler-Illia and M. Takahashi, *J. Sol-Gel Sci. Technol.*, 2019, **89**, 216–224.
- 21 N. Tarutani, Y. Tokudome, M. Jobbágy, G. J. A. A. Soler-Illia, Q. Tang, M. Müller and M. Takahashi, *Chem. Mater.*, 2019, **31**, 322–330.
- 22 S. Rey, J. Mérida-Robles, K.-S. Han, L. Guerlou-Demourgues, C. Delmas and E. Duguet, *Polym. Int.*, 1999, **48**, 277–282.
- 23 C. Vaysse, L. Guerlou-Demourgues, E. Duguet and C. Delmas, *Inorg. Chem.*, 2003, **42**, 4559–4567.
- 24 F. Song and X. Hu, *Nat. Commun.*, 2014, **5**, 1–9.
- 25 N. Tarutani, Y. Tokudome, M. Fukui, K. Nakanishi and M. Takahashi, *RSC Adv.*, 2015, **5**, 57187–57192.
- 26 J. Liang, M. Renzhi, N. Iyi, Y. Ebina, K. Takada and T. Sasaki, *Chem. Mater.*, 2010, **22**, 371–378.
- 27 N. S. McIntyre and M. G. Cook, *Anal. Chem.*, 1975, **47**, 2208–2213.
- 28 C. V. Schenck, J. G. Dillard and J. W. Murray, *J. Colloid Interface Sci.*, 1983, **95**, 398–409.
- 29 J. Ismail, M. F. Ahmed and P. Vishnu Kamath, *J. Power Sources*, 1991, **36**, 507–516.
- 30 P. Oliva, J. Leonardi, J. F. Laurent, C. Delmas, J. J. Braconnier, M. Figlarz, F. Fievet and A. de Guibert, *J. Power Sources*, 1982, **8**, 229–255.
- 31 Z. A. Hu, Y. L. Xie, Y. X. Wang, H. Y. Wu, Y. Y. Yang and Z. Y. Zhang, *Electrochim. Acta*, 2009, **54**, 2737–2741.
- 32 L. Xie, Z. Hu, C. Lv, G. Sun, J. Wang, Y. Li, H. He, J. Wang and K. Li, *Electrochim. Acta*, 2012, **78**, 205–211.
- 33 X. Liu, R. Ma, Y. Bando and T. Sasaki, *Adv. Mater.*, 2012, **24**, 2148–2153.
- 34 X. Zheng, Z. Gu, Q. Hu, B. Geng and X. Zhang, *RSC Adv.*, 2015, **5**, 17007–17013.
- 35 J. Ismail, M. F. Ahmed and P. Vishnu Kamath, *J. Power Sources*, 1993, **41**, 223–230.
- 36 M. E. Folquer, J. R. Vilche and A. J. Arvia, *J. Electroanal. Chem. Interfacial Electrochem.*, 1984, **172**, 235–253.
- 37 J. Li, M. Yang, J. Wei and Z. Zhou, *Nanoscale*, 2012, **4**, 4498.
- 38 C. Nethravathi, N. Ravishankar, C. Shivakumara and M. Rajamathi, *J. Power Sources*, 2007, **172**, 970–974.
- 39 M. Sebastian, C. Nethravathi and M. Rajamathi, *Mater. Res. Bull.*, 2013, **48**, 2715–2719.
- 40 B. Schneiderová, J. Demel, A. Zhigunov, J. Bohuslav, H. Tarábková, P. Janda and K. Lang, *J. Colloid Interface Sci.*, 2017, **499**, 138–144.
- 41 R. D. Armstrong, G. W. D. Briggs and E. a. Charles, *J. Appl. Electrochem.*, 1988, **18**, 215–219.
- 42 R. D. Armstrong and E. A. Charles, *J. Power Sources*, 1989, **25**, 89–97.
- 43 W.-L. Hong and L.-Y. Lin, *J. Power Sources*, 2019, **435**, 226797.
- 44 K.-L. Chiu and L.-Y. Lin, *J. Mater. Chem. A*, 2019, **7**, 4626–4639.
- 45 K.-C. Ho and L.-Y. Lin, *J. Mater. Chem. A*, 2019, **7**, 3516–3530.
- 46 T. Löffler, A. Savan, A. Garzón-Manjón, M. Meischein, C. Scheu, A. Ludwig and W. Schuhmann, *ACS Energy Lett.*, 2019, **4**, 1206–1214.